

Nanoscale Liquid Crystal Lubrication Controlled by Surface Structure and Film Composition

Pritam Kumar Jana^{1,*}, Wei Chen², Mikko J. Alava¹, and Lasse Laurson^{1†}

¹*COMP Centre of Excellence, Department of Applied Physics,*

Aalto University, P.O.Box 11100, FI-00076 Aalto, Espoo, Finland and

²*State Key Laboratory of Multiphase Complex Systems, Institute of Process Engineering (IPE), Chinese Academy of Sciences (CAS), Beijing 100190, PR China.*

Liquid crystals have emerged as potential candidates for next-generation lubricants due to their tendency to exhibit long-range ordering. Here, we construct a full atomistic model of 4-cyano-4-hexylbiphenyl (6CB) nematic liquid crystal lubricants mixed with hexane and confined by mica surfaces. We explore the effect of the surface structure of mica, as well as lubricant composition and thickness, on the nanoscale friction in the system. Our results demonstrate the key role of the structure of the mica surfaces, specifically the positions of potassium (K^+) ions, in determining the nature of sliding friction with monolayer lubricants, including the presence or absence of stick-slip dynamics. With the commensurate setup of confining surfaces, when the grooves created between the periodic K^+ ions are parallel to the sliding direction we observe a lower friction force as compared to the perpendicular situation. Random positions of ions exhibit even smaller friction forces with respect to the previous two cases. For thicker lubrication layers the surface structure becomes less important and we observe a good agreement with the experimental data on bulk viscosity of 6CB and the additive hexane. In case of thicker lubrication layers, friction may still be controlled by tuning the relative concentrations of 6CB and hexane in the mixture.

I. INTRODUCTION

Controlling friction, wear, and lubrication by understanding the atomic-scale processes taking place at the interfaces of interacting bodies in relative motion has been a long-standing challenge, with applications, for example, in micro- and nanoelectromechanical systems [1–3]. Many classical laws of friction and lubrication in such systems are violated due to the high surface-to-volume ratio and the greater importance of molecular interactions and arrangements in determining the surface forces [4]. As a result, a number of fundamental questions in this field are still unsolved [5].

A practical design goal for applications is to reduce stiction, friction and wear. To this end, one may think of two main strategies: either modulating the roughness, electrostatic interactions, crystal structure, edge orientations and other properties of the surfaces that come into contact or by using various types of lubricants between the surfaces [6, 7]. Approaches with the idea of tuning the potential energy landscape between the interacting surfaces at the atomic scale have been proposed [6], including the use of aperiodic quasicrystal surfaces or introducing a lattice mismatch between the two sliding crystal surfaces, leading to the superlubricity mechanism [2, 8, 9]. However, a recent study shows that the duration of the superlubric state, i.e., the incommensurate configuration can be finite and therefore, ultralow friction does not prevail. The possibility of rotation of the sliding surface stabilizes the high frictional commensurate

configuration [10, 11]. The idea of aligning the crystallographic orientation of confining layers is used in resonant tunneling diodes [12] and other novel devices [11]. It suggests to perform more investigations on reducing friction considering energetically stabilized high frictional commensurate setup. Guo et al. have shown that interlayer friction, in case of commensurate setup, can be reduced by functionalizing the sliding surfaces [13]. Several studies have been performed focusing on the quest of perfect lubricants and their dynamical properties or the adsorbate surface coverage while being sheared by the confining surfaces in relative sliding motion [1, 14–16].

Liquid crystals (LCs) have been explored as potential lubricant due to ultra-low friction as a result of their long-range orientational ordering tendency [17]. Due to the high cost of pure LCs, various mixtures of LCs with other substances are typically considered, and more extensive investigations are required to understand the effects due to such additives [18–22]. There are open questions related to details of the interactions of the LC molecules with the confining surfaces, and the phase behavior they exhibit under applied shear. While experiments, coarse-grained simulations, and theoretical studies to understand the structural and dynamical properties of LC lubricants have been performed [18, 22–32], atomistic simulations to establish a proper link between coarse-grained models and experiments are still missing.

In this article, we focus on the lubricating properties of nematic 4-cyano-4-hexylbiphenyl (6CB) LCs in pure and in presence of hexane additives where mica serves as confining surfaces by using fully atomistic model simulations. We probe the influence of the relative orientation of the surfaces including an incommensurate setup, and the effect of the random ion distribution in the confining mica surfaces. We also inspect the impact of the thickness of

* pritam.jana@aalto.fi

† lasse.laurson@aalto.fi

the lubricant film, whether pure 6CB or a 6CB/hexane mixture, on frictional response. Our results show that friction in systems with monolayer lubricant films is sensitive to the arrangement of ions on the confining surfaces or to the relative surface orientations. Moreover, we demonstrate friction control also for thicker lubricant layers via tuning the composition of the LC-hexane mixture, including controlling the presence of stick-slip.

II. MODEL

There are several efforts to reproduce the properties, for example, the so-called odd-even effect in nematic-isotropic transition, of liquid crystal homologues namely 4-cyano-4-alkylbiphenyl (nCB) up to a satisfactory level of accuracy in computer simulations[33, 34]. In the present study, we are specifically interested in the lubricating properties of liquid crystals because of its long-range ordering. To this end, we choose 4-cyano-4-hexylbiphenyl (6CB). There is experimental evidence on lubrication of 6CB confined between mica surfaces[35–37]. We could have chosen other homologues. However, we believe that the observed results will qualitatively remain same. We consider hexane as an additive because of its low cost and is largely used as a lubricant. To construct the atomistic models of 6CB and hexane molecules, we use force field parameters from Refs. [38, 39]. As for the confining mica surfaces, we consider 2M1-muscovite mica with the formula $\text{KAl}_2(\text{Al,Si}_3)\text{O}_{10}(\text{OH})_2$, using the force field parameters as described in Ref. [40]. Details of the force field parameters used in the simulations are provided in the Supporting Information. To verify the accuracy of the force field, we have calculated two friction related quantities: (a) bulk viscosity for both 6CB liquid crystal and hexane and we see a good agreement with experiments. See the inset of Fig. 3. (b) friction force for commensurate (confining surfaces are aligned) and the incommensurate surface (confining surfaces are misaligned) and we observe a lower friction in case of the incommensurate surface which is also observed in experiments. Both results, we discuss in detail in Results and discussions section. It assures that the used force field parameters are good enough to study frictional properties of 6CB and hexane.

In an experiment, Atomic Force Microscope (AFM) cannot detect potassium ions (K^+) on mica surfaces. A probable reason of that is K^+ ions on mica are moved around by the AFM cantilever-tip during the sliding motion[41]. However, there are several efforts on understanding the spatial arrangement of ions at the solid-liquid interface. Ricci et al. have shown that the monovalent metal ions do not adsorb on mica surfaces immersed in water randomly but form preferential ordered structures to minimize the surface energy at the mica-ion interface[42]. Most of the theoretical studies consider the periodic arrangement of K^+ ions[43]. However, due to the randomness of the cleaving process of mica,

uniform distribution of K^+ ions is unlikely[44]. Those experimental observations lead us to consider both periodic and random arrangements of K^+ ions and examine the resulting effects on friction. Each surface consists of 10×6 unit cells and linear dimensions of $L_x = 103.76$ Å and $L_y = 70.54$ Å, respectively. Both surfaces are kept parallel to the xy plane, and the upper surface is driven with a constant velocity of $V = 0.1$ m/s along the x direction. We do not consider the y directional motion of any of the plates. As shown in Fig. 1(a), the lower surface is attached to a fixed point with a spring constant $k/N_p = 0.007$ N/m, with N_p the number of atoms in the surface which is a basic tribological setup [45]. The spring constant is consistent with experimental values as mentioned in Refs. [46, 47] and the sliding velocity (here 0.1m/s) of the upper plate is smaller than the critical velocity defined as the limiting velocity after which stick-slip motion disappears [48]. Therefore, under the chosen values of parameters, we expect stick-slip dynamics in the system with thin layer of lubricants so that in addition to study the frictional effect of ions position on mica surfaces, we can also characterise the dynamical behavior of nano-confined liquid crystals during the stick and the slip events.

In the steady state, the upper surface is subject to a normal load corresponding to a 1 atm. We do not vary normal load. However, it could be an interesting direction to explore the responses of nanoscale friction for different normal loads that usually disobey a simple linear relation[5]. Temperature of the lubricants is maintained at $T = 298$ K using a Langevin thermostat, applied only in the y direction to avoid streaming bias [14, 49, 50]. To make sure that thermostat does not affect our main results, we use the temperature relaxation time 10^{-4} ns which is significantly smaller than the time required ($\sim 10^{-2}$ ns) to finish a slip event. The equations of motion are solved with the velocity Verlet algorithm implemented in the LAMMPS code[51], with an integration time step of 1 fs. Long-range electrostatic interactions are computed by using the particle-particle-particle-mesh solver for the slab geometry [52, 53] with 10^{-4} accuracy [54] implemented in LAMMPS[51]. Initially lubricant molecules are arranged in a simple cubic lattice and first equilibrate for 100 ps with both confining surfaces fixed. During the following 100 ps, the top surface is subject to a normal load corresponding to a 1 atm pressure and is allowed to move along the z direction. After that, the top surface is driven along the x axis with a velocity V for 60 ns; in most cases the observables of interest have been averaged over the last 20 ns of the simulations, to ensure that a steady state is reached.

III. RESULTS AND DISCUSSIONS

We divide our results into two subsections. First, we discuss the effects of surface structure and orientation on friction. Next, we show how additives' concentration can

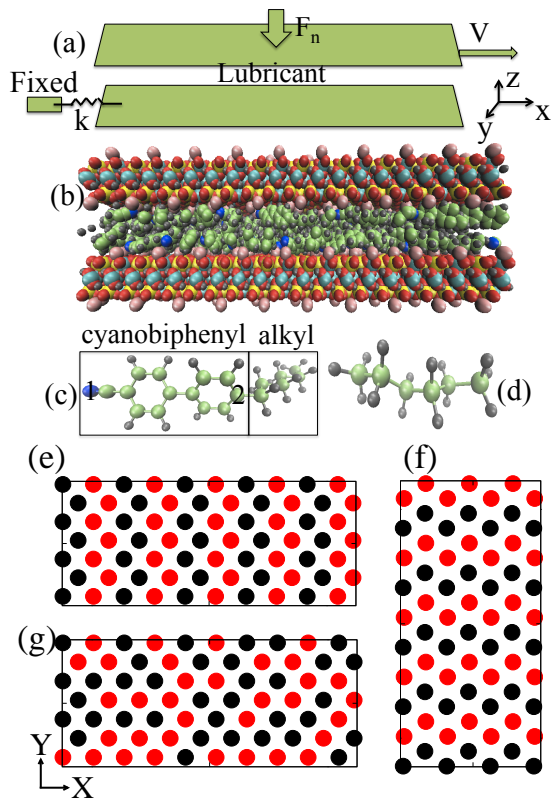


FIG. 1. (a) A schematic of the model. Lower plate is attached with a spring to a fixed point. The upper surface is subject to a normal load F_n and driven along the $+x$ direction with a constant velocity V . (b) A snapshot of the system is depicted, with 144 6CB molecules confined by the two mica plates. (c) and (d) correspond to the molecular structures of 6CB (consisting of cyanobiphenyl and alkyl groups) and hexane, respectively. Pink, red, yellow, cyan, green, grey and blue colored atoms are potassium, oxygen, silicon, aluminum, carbon, hydrogen and nitrogen, respectively. (e), (f) and (g) show the different arrangements of the K^+ ions at the surfaces considered in the simulations (only a small part of the surface shown, with red and black dots corresponding to upper and lower faces of the mica sheet, respectively), i.e., with grooves perpendicular and parallel to the sliding direction, and a random arrangement of the ions, respectively.

tune the resulting friction forces.

A. Effects of surface structure and orientation on friction

As we are interested in understanding the boundary lubrication, where friction between the confining surfaces depends on the surface properties and the properties of the thin layer of lubricants, first we consider the system with monolayer of 6CB and hexane molecules. For the system geometry considered here, monolayer systems are obtained by considering 72 6CB or 144 hexane molecules, respectively. To construct a monolayer we choose the number of molecules to be such that the total area oc-

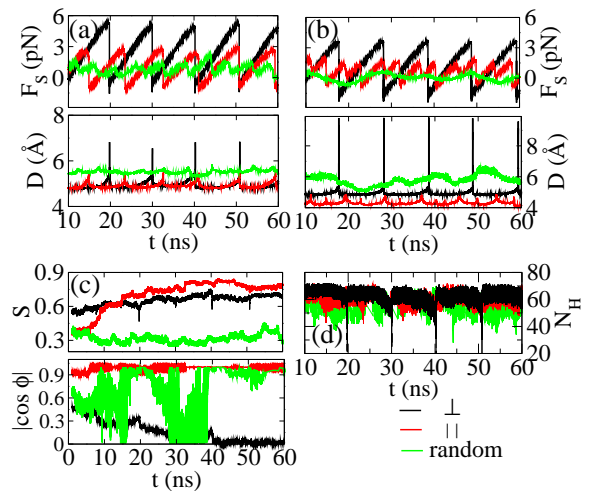


FIG. 2. Time evolution of the friction force F_s and film thickness D for monolayers of (a) 6CB and (b) hexane, considering the three different arrangements of the K^+ ions at the surfaces depicted in Fig. 1. (c) Order parameter S and the angle ϕ between the 6CB director and the sliding direction, quantified here by $\cos \phi$, are shown in the top and the bottom panel, respectively. (d) Time evolution of the number N_H of hydrogen bonds between the 6CB and bottom mica, illustrating that the bonds tend to break during the slip events.

cupied by them is smaller than the area of the confining surfaces. To characterize the dynamics, we compute the friction force F_s (the average force exerted on each atom of the bottom plate by the lubricant and the top mica plate along the $+x$ direction), film thickness D (distance between the two plates), and the order parameter S of the LCs, i.e., the maximum eigenvalue of the average ordering tensor $Q_{\alpha,\beta}$ defined as

$$Q_{\alpha,\beta} = \frac{1}{N} \sum_i \left(\frac{3}{2} u_\alpha^i u_\beta^i - \frac{1}{2} \delta_{\alpha,\beta} \right), \quad (1)$$

where u_α^i ($\alpha, \beta = x, y, z$) are the Cartesian components of the unit vector of the LC molecule i , N is the number of LC molecules, and $\delta_{\alpha,\beta}$ is the Kronecker delta. Here, the unit vector of the LC molecule is taken to be parallel to the line connecting the nitrogen atom and the end carbon of the cyanobiphenyl group of 6CB, denoted by 1 and 2 in Fig. 1(c), respectively. We also compute the director (eigenvector of the maximum eigenvalue) of the LC molecules (the average molecular orientation), and characterize it by the angle ϕ with the x -axis.

The monolayer results are summarized in Fig. 2, considering three different arrangements of the K^+ ions on the mica surfaces: Figs. 1(e) and (f) display two different periodic arrangements of the ions [the structure in (f) is obtained by rotating the surface in (e) by 90°], while Fig. 1(g) shows an example with randomly positioned ions. It is important to notice that in the case of the two periodic arrangements, grooves are generated along the x [Fig. 1(f)] or y direction [Fig. 1(e)] in between stripes of ions,

resulting in an anisotropic surface structure, while in the case of randomly positioned ions, such features are absent [Fig. 1(g)]. To examine the effect of surface structure on boundary lubricated friction, we plot in Figs. 2 (a) and (b) the time-dependence of the friction force F_s and the film thickness D for those three different structures of the confining mica surfaces for 6CB and hexane, respectively; see also example movies (Videos SM1, SM2, and SM3) provided as Supporting Information. We observe regular stick-slip dynamics for both 6CB and hexane for the ordered surfaces. The maximum friction force (and thus the magnitude of the stick-slip oscillations) as well as the maximum film thickness during the “jumps” of the top plate associated with the slip events are larger in the case where the grooves of the mica surfaces are perpendicular to the sliding direction. In case of 6CB lubricated system, this effect is visible also when considering the time evolution of the number of hydrogen bonds, N_H , formed between 6CB hydrogens and the bottom mica plate (i.e., the number of 6CB hydrogens closer than 3 Å from the bottom mica surface [50]. A typical hydrogen bond length is 1.5 Å to 2.5 Å which is smaller than the distance, 3 Å, that we consider as the breakage of hydrogen bonds.), see Fig. 2 (d): bonds break as the system evolves from stick to the slip state. In the case of the randomly positioned ions, 6CB exhibits more irregular stick-slip dynamics, with also some visible jumps in D accompanying the slip events, while no clear signature of stick-slip is observed for hexane. Due to the incommensurate nature of the confining surfaces with randomly positioned K^+ ions, the average film thickness D is larger and the maximum F_s is lower than with ordered mica surfaces. A similar observation is depicted in an experiment where surface ion induced tribological properties have been studied. It has been shown that when the ions are strongly bound and randomly distributed on mica irregular stick-slip occurs [41]. Several experimental studies have been performed to understand the dynamical or mechanical properties of organic liquids when they are confined to few layers by solid surfaces such as mica [55]. A common phenomenon is the observation of stick-slip motion depending on the sliding velocity and the normal load [56, 57]. Although there are several efforts, molecular origin of stick-slip cycle in sheared solid-like lubricants is not well understood because of the difficulties to capture the behaviour of lubricants during the slip events, precisely mainly for two reasons: (a) slip events occur in nanometrically confined film (b) slip events are of very short duration and occupy a tiny fraction of the stick-slip cycle [57]. Therefore, a lot of understanding has been derived from theoretical and computer simulations. To this end, we also explore the behaviour of confined LCs during the stick and the slip events.

For 6CB LCs, the time-evolution of the order parameter S and the angle ϕ between the LC director and the sliding direction (x axis) [Fig. 2 (c)] encode additional information about the dynamics. In particular, 6CBs have a tendency to orient along both the grooves of the confin-

ing surfaces (due to formation of hydrogen bonds between the biphenyl hydrogen and the surface oxygen exposed along the grooves), as well as along the sliding direction: S is larger and ϕ is smaller when the grooves and the sliding direction are parallel [both along x , see Fig. 1(f)]. For the perpendicular case, in the steady state the 6CBs point mostly along y (i.e., along the grooves), but S is a little smaller than in the parallel case due to the competing ordering mechanism of the sliding along x . It shows that the monolayer of LCs prefers to orient along the microgrooves instead of aligning along the sliding direction due to the presence of strong chemical interactions. In contrast, for the random arrangement of K^+ ions on mica, the 6CBs exhibit clearly less orientational order (smaller S), and ϕ also fluctuates significantly in time, see Fig. 2 (c). The alignment of LCs along the grooves is not a complete surprise. Vegt et al. have investigated the orientation of 4-cyano-4-octylbiphenyl (8CB) liquid crystals on anisotropic polyimide surfaces by performing molecular dynamics simulations where they have shown that a single molecule of 8CB prefers to orient along the microgrooves because of the strong binding between polar cyano groups from LCs and the carbonyl groups from the polyimide surface[58]. In general, understanding the orientation of LCs on the surface is interesting because of its application in liquid crystal display.

To explore more about the dynamics of LCs and their response during the stick-slip cycle we measure the mean square displacement (MSD) of 6CB molecules. It shows that while the molecules move ballistically along x for time scales longer than the stick-slip period for all mica surface structures (Fig. SM2 (a) in the Supporting Information) they exhibit diffusive dynamics in the y direction in the long-time limit only for random ion arrangement and grooves perpendicular to the sliding direction (Fig. SM2 (c) in the Supporting Information). In contrast, for grooves parallel to the sliding direction, MSD saturates to a value comparable to the groove spacing, suggesting that in that case the grooves act as barriers for the y -directional diffusion of 6CBs. However, the slip is confined to the lubricant close to the lower plate, and happens in the direction of sliding. Details are shown in the Supporting Information. Thus, for monolayer lubricants, the structure of the confining surfaces plays a decisive role in the frictional response. So far, we have discussed the system where confining surfaces are aligned with each other- thus commensurate. When we consider the incommensurate setup, i.e, two surfaces are misaligned with respect to each other, we see a frictional response which is even somewhat lower than the situation where K^+ ions are randomly positioned on the surface. See Fig. SM7 in the Supporting Information. Experiments show the similar observations as misaligned mica surfaces exhibit lower friction forces as compared to the commensurate setup [8, 9].

To understand the effect of the confining films' thickness on friction, we study here the periodic pattern of the K^+ ions with the grooves perpendicular to the sliding di-

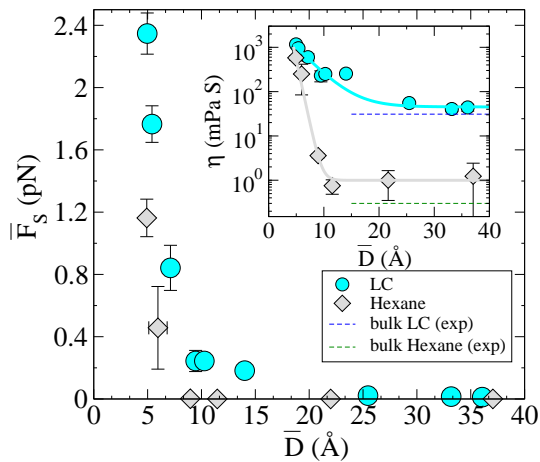


FIG. 3. Average friction force \bar{F}_s as a function of the average film thickness \bar{D} , obtained by considering different numbers of molecules confined by the mica surfaces, with the film consisting of pure 6CB or pure hexane. The inset shows the corresponding dynamic viscosities η , which approach in both cases the experimental bulk viscosity values (Refs. [59, 60] and [61] for 6CB and hexane, respectively), indicated by the dashed horizontal lines. Solid lines are fits of the form of $\eta(\bar{D}) \propto \exp(-\bar{D}/\lambda) + \eta_0$, yielding $\lambda = 0.73 \text{ \AA}$ and 3.36 \AA for hexane and 6CB, respectively.

rection; for thicker lubricant films, stick-slip dynamics gradually disappears with increasing D (see Fig. SM3 in the Supporting Information), and the surface structure of mica becomes less important, with all the three surface structures from above yielding similar results for the friction force. A similar observation is reported when water is confined between mica surfaces [50]. We consider various systems with the number of 6CBs ranging from 72 to 600, and the number of hexane molecules from 144 to 640, and also systems with a smaller area of the confining mica plates to reach a larger D for a given number of lubricant molecules. We compute the resulting average friction force \bar{F}_s as a function of the average thickness \bar{D} (Fig. 3; see also Supporting Information Video SM4 for an example movie of a thick 6CB system). The inset of Fig. 3 displays the corresponding dynamic viscosities η , defined via $\bar{F}_s N_p = \eta A(V/\bar{D})$, where A is the surface area [62]. Under strong confinement (small \bar{D}), both systems exhibit a high dynamic viscosity which decreases with increasing \bar{D} , and approaches the known bulk viscosity values at $T = 298 \text{ K}$, i.e., 31.3 and 0.3 mPa.s for 6CB [59, 60] and hexane [61], respectively. Notice that in general η is expected to depend on V (or the shear rate) [63], but our results indicate that $V = 0.1 \text{ m/s}$ is a sufficiently low sliding velocity such that η approaches a value close to that of the bulk viscosity in the limit of large \bar{D} . We fit the data by $\eta(\bar{D}) \propto \exp(-\bar{D}/\lambda) + \eta_0$, yielding a decay length $\lambda = 0.73 \text{ \AA}$ and 3.36 \AA for hexane and 6CB, respectively. This slower approach to bulk behavior for 6CBs may be understood via the competition between screening of the mica-mica interaction and the

inherent “stickiness” of the 6CB lubricant, with the latter manifested also as the higher bulk viscosity value for 6CB. Due to their larger dielectric constant ($\epsilon \approx 9.5$ for 6CB [64] vs $\epsilon \approx 1.88$ for hexane [65]), one would expect 6CBs to be more efficient at screening the electrostatic interaction between the mica plates [66]. However, at the same time, the sticky nature of 6CB molecules, originating from the Coulomb interaction of the positively charged mica K^+ ions and the highly electronegative nitrogen atoms, as well as from the hydrogen bonding between phenyl hydrogen and mica oxygen atoms, hinders the rapid reduction of friction as \bar{D} increases. The difference in the screening properties of the two lubricants can also be seen by noticing that $\eta_{bulk}^{LC}/\eta_{bulk}^H \approx 35.8$, while in the monolayer case $\eta_{LC}/\eta_H \approx 2$ (with η_{bulk}^{LC} and η_{bulk}^H the measured η -values of LCs and hexane, respectively), suggesting (in relative terms) a stronger surface-surface interaction through a thin layer of hexane as compared to the LC case. We note that a similar evolution with \bar{D} of the viscosity of LC lubricants has been observed experimentally [67]. The MSD of the 6CB molecules shows that in thicker systems they exhibit ballistic motion along x and diffusive dynamics in the y direction independent of the structure of the confining surfaces (Figs. SM2 (b) and (d) in the Supporting Information).

We also investigate the molecular orientation for thicker lubrication films. In contrast to the monolayer case with grooves perpendicular to the sliding direction (see Fig. 1 (e)), we observe that the director fields for thicker LC films tend to orient along the sliding motion as shown in Fig. SM5 (a) in the Supporting Information. Due to larger distances between the confining plates, they also display a z -directional degree of freedom which is absent in the monolayer cases, see Fig. SM5 (b) in the Supporting Information. We do not see homeotropic alignment, i.e., a perpendicular arrangement with respect to the confining surfaces. Experiments also exhibit that in case of untreated mica, LCs have a tendency to be in the plane of the surface [68]. In these studies of LCs as a lubricant we have not paid any direct attention to the general structural properties of the LC films. This concerns both eventual smectic order in thicker systems (and the corresponding dislocations) and the point defects or disclination lines in the presence of nematic order depending on the lubrication layer thickness.

B. Effect of film composition on friction

Finally, to explore the potential film composition of LCs and hexane mixtures at which a reduced friction can be observed, we add various concentrations of hexane to the LC lubricant and compute the friction forces for different mixtures of 6CB LCs and hexane, see Fig. 4 (a). We fix the total number of molecules N to 144, and vary the fraction $\rho_H = N_H/N$ of hexane from 0 to 1, where N_H is the number of hexane molecules. Interestingly, the average friction force \bar{F}_s displays a non-monotonic depen-

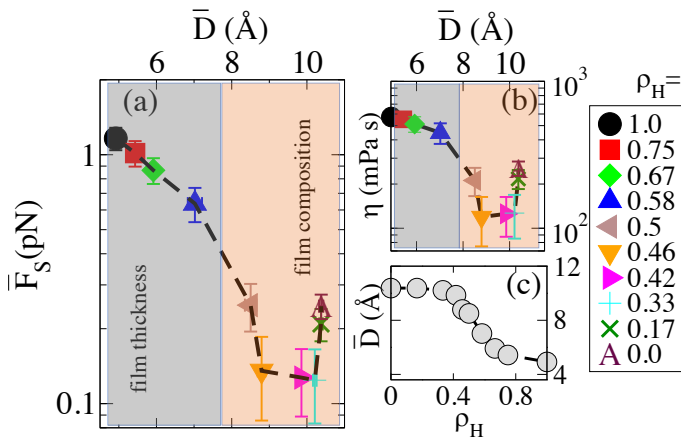


FIG. 4. (a) Average friction force \bar{F}_s as a function of the film thickness \bar{D} for films with different mixtures of 6CB and hexane. (b) shows the corresponding dynamic viscosity η , while (c) displays the film thickness as a function of the hexane concentration ρ_H

dence on ρ_H (and on \bar{D}). While the general trend is that \bar{F}_s decreases with decreasing ρ_H and increasing \bar{D} , for the smallest ρ_H (corresponding to the pure and almost pure LC cases), \bar{F}_s increases with decreasing ρ_H and increasing \bar{D} . As LCs are larger in size and stickier in nature as

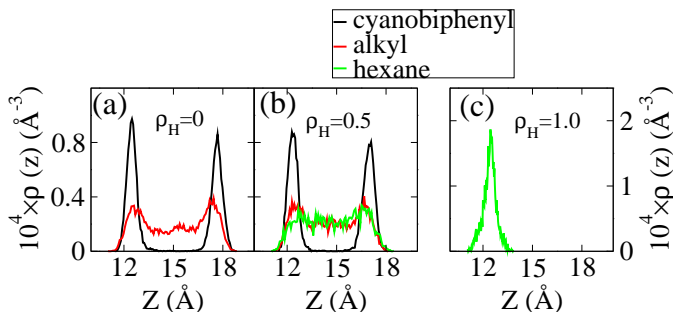


FIG. 5. Probability density profiles $\rho(z)$ describing the probability per unit volume of finding a molecule with a given z coordinate, for 6CB (shown separately for cyanobiphenyl and alkyl groups) and hexane for three different mixtures, (a) 144 pure 6CB, (b) 72 6CB and 72 hexane mixture, and (c) 144 pure hexane. The cyanobiphenyl groups of the 6CBs tend to stay adjacent to the confining mica plates, while the 6CB alkyl groups as well as hexane occupy the space also in the middle of the gap.

compared to hexane, reduction of ρ_H or addition of LCs in the LC-hexane mixture renders a competing effect on friction. A larger size of LC will lead to the thickening of the film and thus decrease of friction while the stickier nature will oppose the effect. When $\rho_H = 1$, hexane is confined to a monolayer between mica surfaces (see Fig. 5 (c)) and stick-slip motion is observed as shown in Fig. 2 (b), thus high friction. With the addition of LCs up to 1:1 ratio, film thickness increases as shown in Fig. 4 (c) and friction decreases rapidly (see Fig. 4 (a)) because

of the gradual disappearance of stick-slip. See Fig. SM4 and Video SM5 in the Supporting Information. Thus, film thickness dominates on controlling the friction. Note that, when $N_{LC} : N_H = 1 : 1$ (N_{LC} is the number of LCs) probability density of the confined mixtures along the z direction exhibits the formation of two layers (See Fig. 5 (b)). Due to the strong attractive interaction between cyanobiphenyl group of 6CB and mica (K^+ ions and oxygens), cyanobiphenyl groups are attracted to the mica surfaces while alkyl parts as well as hexane occupy the space in the middle in between the confining surfaces as shown in Fig. 5 (b). Further addition of LCs leads to the weak changes of thickness and in that region, sticky nature of LCs plays a key role and thus a gradual increase of friction. Density profile $\rho(z)$, when $\rho_H = 0$, exhibits similar probability distribution as observed when $\rho_H = 0.5$. See Fig. 5 (a). The same non-monotonic behavior is visible in the corresponding dynamic viscosity η [Fig. 4 (b)]. In precise, this non-monotonic behavior of friction is a result of the cross-over from a *film thickness* controlled friction regime (shown in Fig. 4(a) as a gray region; in this regime we observe gradual disappearance of stick-slip dynamics with decreasing ρ_H) to a *film composition* dependent regime (orange colored region; stick-slip not observed due to larger \bar{D}). When we characterize the slip at surface depending on the amount of hexane, we see that both slip length and slip position increase as we approach the pure hexane case (See Fig. SM10 in the Supporting Information). The slip in confined LCs follows the surface-slip coherently. However, slip length at surface is larger as compared to the LCs. When the slip length at the surface is small, we do not see any slip in the LCs (See Fig. SM9 in the Supporting Information).

IV. CONCLUSIONS

To summarize, we have presented an extensive study of nanoscale LC lubrication using a full atomistic model. In the boundary lubricated regime we show that nanoscale friction can be tuned by controlling the distribution of ion positions on muscovite mica. In case of commensurate setup, when ions are periodic we observe a larger friction force as compared to the case where ions are randomly placed on mica. In the latter case, the director field of the confined LCs fluctuates while in the former case, director field orients along the grooves created between periodically arranged ions. When grooves and the sliding direction are parallel, LCs exhibit higher order and the friction is lower as compared to the perpendicular case. In case of incommensurate setup, the friction force is smaller than the commensurate setup where ions are randomly arranged on mica and the confined LCs orient along the sliding direction. Tuning the charge distribution and modifying the surface geometry, one can reduce the friction in commensurate structures [13]. The experimental probe of the ion arrangement [44] can open up novel directions in controlling nanoscale fric-

tion. However, at the limit of a large thickness, surface effects disappear and we predict that effective viscosity of the confined LC and hexane exponentially decays to the bulk viscosity that exhibits a good agreement with experimental values.

On the quest of potential lubricant from LC-hexane mixtures, our results show that increase of LC and hexane concentration in the hexane [69] and the liquid crystal dominated regions, respectively both lead to the reduction of friction. It suggests that instead of pure LCs addition of impurity results better lubrication and it can be thought of potential lubricant in applications. By tuning the film composition, we also observe the possibility of controlling the stick-slip motion which is a major reason of wear in sliding surfaces.

ACKNOWLEDGEMENT

PKJ, MJA and LL are supported by the Academy of Finland through project no. 251748 (Centres of Excel-

lence Programme, 2012-2017). PKJ acknowledges support from the Academy of Finland FiDiPro program, project no. 13282993. LL acknowledges the support of the Academy of Finland via an Academy Research Fellowship (project no. 268302). WC is grateful to the financial support by the National Natural Science Foundation of China (Grant No. 11504384). We acknowledge the computational resources provided by the Aalto University School of Science “Science-IT” project, as well as those provided by CSC (Finland). We thank Jens Smittek for useful discussions and suggestions.

-
- [1] B. Bhushan, J. N. Israelachvili, and U. Landman, *Nature* **374**, 607 (1995).
- [2] J. Y. Park, D. F. Ogletree, M. Salmeron, R. A. Ribeiro, P. C. Canfield, C. J. Jenks, and P. A. Thiel, *Science* **309**, 1354 (2005).
- [3] B. Bhushan, *Wear* **259**, 1507 (2005).
- [4] A. M. Smith, K. R. J. Lovelock, N. N. Gosvami, T. Welton, and S. Perkin, *Phys. Chem. Chem. Phys.* **15**, 15317 (2013).
- [5] M. Urbakh, J. Klafter, D. Gourdon, and J. Israelachvili, *Nature* **430**, 525 (2004).
- [6] J. Frenken, *Nat. Nanotechnol.* **1**, 20 (2006).
- [7] H. Zhang and T. Chang, *Nanoscale* **10**, 2447 (2018).
- [8] A. E. Filippov, A. Vanossi, and M. Urbakh, *Phys. Rev. Lett.* **104**, 074302 (2010).
- [9] M. Hirano, K. Shinjo, R. Kaneko, and Y. Murata, *Phys. Rev. Lett.* **67**, 2642 (1991).
- [10] A. E. Filippov, M. Dienwiebel, J. W. M. Frenken, J. Klafter, and M. Urbakh, *Phys. Rev. Lett.* **100**, 046102 (2008).
- [11] C. R. Woods, F. Withers, M. J. Zhu, Y. Cao, G. Yu, A. Kozikov, M. Ben Shalom, S. V. Morozov, M. M. van Wijk, A. Fasolino, M. I. Katsnelson, K. Watanabe, T. Taniguchi, A. K. Geim, A. Mishchenko, and K. S. Novoselov, *Nature Communications* **7**, 10800 (2016).
- [12] A. Mishchenko, J. S. Tu, Y. Cao, R. V. Gorbachev, J. R. Wallbank, M. T. Greenaway, V. E. Morozov, S. V. Morozov, M. J. Zhu, S. L. Wong, F. Withers, C. R. Woods, Y.-J. Kim, K. Watanabe, T. Taniguchi, E. E. Vdovin, O. Makarovskiy, T. M. Fromhold, V. I. Fal’ko, A. K. Geim, L. Eaves, and K. S. Novoselov, *Nature Nanotechnology* **9**, 808 (2014).
- [13] Y. Guo, J. Qiu, and W. Guo, *Nanoscale* **8**, 575 (2016).
- [14] P. A. Thompson and S. M. Troian, *Nature* **389**, 360 (1997).
- [15] M. A. Zaidan, F. F. Canova, L. Laurson, and A. S. Foster, *J. Chem. Theory Comput.* **13**, 3 (2016).
- [16] W. Ouyang, A. S. de Wijn, and M. Urbakh, *Nanoscale* **10**, 6375 (2018).
- [17] T. Amann and A. Kailer, *Tribol. Lett.* **37**, 343 (2010).
- [18] C. Manzato, A. S. Foster, M. J. Alava, and L. Laurson, *Phys. Rev. E* **91**, 012504 (2015).
- [19] E. Strelcov, R. Kumar, V. Bocharova, B. G. Sumpter, A. Tselev, and S. V. Kalinin, *Sci. Rep.* **5**, 8049 EP (2015).
- [20] H.-W. Hu, G. A. Carson, and S. Granick, *Phys. Rev. Lett.* **66**, 2758 (1991).
- [21] S. Nakano, M. Mizukami, and K. Kurihara, *Soft Matter* **10**, 2110 (2014).
- [22] W. Chen, S. Kulju, A. S. Foster, M. J. Alava, and L. Laurson, *Phys. Rev. E* **90**, 012404 (2014).
- [23] F.-J. C.-V. Mara-Dolores Bermudez, Gins Martnez-Nicols, *Wear* **212**, 188 (1997).
- [24] F. C. G. M.-N. P. Iglesias, M.D. Bermudez, *Wear* **256**, 386 (2004).
- [25] F.-J. Carrion, G. Martnez-Nicolas, P. Iglesias, J. Sanes, and M.-D. Bermudez, *Int. J. Mol. Sci.* **10**, 4102 (2009).
- [26] M. Ruths, S. Steinberg, and J. N. Israelachvili, *Langmuir* **12**, 6637 (1996).
- [27] L. Noirez, G. Ppy, and P. Baroni, *J. Phys. Condens. Matter* **17**, S3155 (2005).
- [28] R. J. Bushby and K. Kawata, *Liq. Cryst.* **38**, 1415 (2011).
- [29] C. Pujolle-Robic and L. Noirez, *Phys. Rev. E* **68**, 061706 (2003).
- [30] S. H. Idziak, C. R. Safinya, R. S. Hill, K. E. Kraiser, M. Ruths, H. E. Warriner, S. Steinberg, K. S. Liang, and J. N. Israelachvili, *Science* **264**, 1915 (1994).
- [31] C. H. A. Cheng, L. H. Kellogg, S. Shkoller, and D. L. Turcotte, *Proceedings of the National Academy of Sciences* **105**, 7930 (2008).

- [32] X. Zhang, X. Zhang, X. Qiao, Y. Guo, Y. Tian, and Y. Meng, *Microfluidics and Nanofluidics* **18**, 1131 (2015).
- [33] M. Cifelli, L. De Gaetani, G. Prampolini, and A. Tani, *The Journal of Physical Chemistry B* **112**, 9777 (2008).
- [34] G. Tiberio, L. Muccioli, R. Berardi, and C. Zannoni, *ChemPhysChem* **10**, 125 (2009).
- [35] J. Janik, R. Tadmor, and J. Klein, *Langmuir* **13**, 4466 (1997).
- [36] V. Kitaev and E. Kumacheva, *The Journal of Physical Chemistry B* **104**, 8822 (2000).
- [37] M. Mizukami, K. Kusakabe, and K. Kurihara, in *Surface and Colloid Science* (Springer, 2004) pp. 105–108.
- [38] C. J. Adam, S. J. Clark, G. J. Ackland, and J. Crain, *Phys. Rev. E* **55**, 5641 (1997).
- [39] D. L. Cheung, S. J. Clark, and M. R. Wilson, *Phys. Rev. E* **65**, 051709 (2002).
- [40] H. Heinz, H. Koerner, K. L. Anderson, R. A. Vaia, and B. L. Farmer, *Chem. Mater.* **17**, 5658 (2005).
- [41] L. Xu and M. Salmeron, *Langmuir* **14**, 2187 (1998).
- [42] M. Ricci, P. Spijker, and K. Vořchovsky, *Nature communications* **5**, 4400 (2014).
- [43] M. Odelius, M. Bernasconi, and M. Parrinello, *Phys. Rev. Lett.* **78**, 2855 (1997).
- [44] P. Bampoulis, K. Sotthewes, M. H. Siekman, H. J. Zandvliet, and B. Poelsema, *Sci. Rep.* **7**, 43451 (2017).
- [45] W. Ouyang, M. Ma, Q. Zheng, and M. Urbakh, *Nano Letters* **16**, 1878 (2016).
- [46] M. Dienwiebel, G. S. Verhoeven, N. Pradeep, J. W. M. Frenken, J. A. Heimberg, and H. W. Zandbergen, *Phys. Rev. Lett.* **92**, 126101 (2004).
- [47] H. Yoshizawa and J. Israelachvili, *The Journal of Physical Chemistry* **97**, 11300 (1993).
- [48] Y. Lei and Y. Leng, *Phys. Rev. Lett.* **107**, 147801 (2011).
- [49] P. A. Thompson and M. O. Robbins, *Phys. Rev. A* **41**, 6830 (1990).
- [50] W. Chen, A. S. Foster, M. J. Alava, and L. Laurson, *Phys. Rev. Lett.* **114**, 095502 (2015).
- [51] S. Plimpton, *Journal of computational physics* **117**, 1 (1995).
- [52] P. A. Patel, J. Jeon, P. T. Mather, and A. V. Dobrynin, *Langmuir* **22**, 9994 (2006).
- [53] C. Pan, S. Yi, and Z. Hu, *Physical Chemistry Chemical Physics* **19**, 4861 (2017).
- [54] J. J. Cerda, B. Qiao, and C. Holm, *Soft Matter* **5**, 4412 (2009).
- [55] E. Kumacheva and J. Klein, *The Journal of chemical physics* **108**, 7010 (1998).
- [56] S. Ohnishi, D. Kaneko, J. P. Gong, Y. Osada, A. M. Stewart, and V. V. Yaminsky, *Langmuir* **23**, 7032 (2007).
- [57] I. Rosenhek-Goldian, N. Kampf, A. Yeredor, and J. Klein, *Proceedings of the National Academy of Sciences* **112**, 7117 (2015).
- [58] N. Van der Vegt, F. Müller-Plathe, A. Geleßus, and D. Johannsmann, *The Journal of Chemical Physics* **115**, 9935 (2001).
- [59] T. Hirano and K. Sakai, *Phys. Rev. E* **77**, 011703 (2008).
- [60] J. Jadzyn, G. Czechowski, and D. Bauman, *Z. Naturforsch. A* **55**, 810 (2000).
- [61] A. Rodríguez, A. Pereiro, J. Canosa, and J. Tojo, *J. Chem. Thermodyn.* **38**, 505 (2006).
- [62] Y. Leng and P. T. Cummings, *Phys. Rev. Lett.* **94**, 026101 (2005).
- [63] A. Jabbarzadeh, P. Harrowell, and R. Tanner, *Phys. Rev. Lett.* **94**, 126103 (2005).
- [64] B. R. Ratna and R. Shashidhar, *Pramana* **6**, 278 (1976).
- [65] F. I. Mopsik, *J. Res. Natl. Bur. Stand. Sec. A* **71 A**, 287 (1967).
- [66] A. A. Lee, C. S. Perez-Martinez, A. M. Smith, and S. Perkin, *Phys. Rev. Lett.* **119**, 026002 (2017).
- [67] M. Shen, J. Luo, S. Wen, and J. Yao, *Chin. Sci. Bull.* **46**, 1227 (2001).
- [68] M. Ruths and S. Granick, *Langmuir* **16**, 8368 (2000).
- [69] B. Kupchinov, V. Rodnenkov, S. Ermakov, and V. Parkalov, *Tribology International* **24**, 25 (1991).

Supporting Information

Force field

For 4-cyano-4-hexylbiphenyl (6CB) liquid crystals the force field has the following functional form

where

$$E_f = E_{stretching} + E_{bending} + E_{torsional} + E_{vdw} + E_{electrostatic} \quad (1)$$

$$E_{stretching} = \sum_{bonds} \frac{1}{2} k_l (l - l_0)^2 \quad (2)$$

$$E_{bending} = \sum_{angles} \frac{1}{2} k_\theta (\theta - \theta_0)^2 \quad (3)$$

$$E_{torsional} = \sum_{dihedrals} \left[\frac{1}{2} k_1 (1 + \cos \varphi_i) + \frac{1}{2} k_2 (1 - \cos 2\varphi_i) + \frac{1}{2} k_3 (1 + \cos 3\varphi_i) + \frac{1}{2} k_4 (1 - \cos 4\varphi_i) \right] \quad (4)$$

$$E_{vdw} = \sum_{i,j} 4\varepsilon_{ij} \left[\left(\frac{\sigma_{ij}}{\varepsilon_{ij}} \right)^{12} - \left(\frac{\sigma_{ij}}{\varepsilon_{ij}} \right)^6 \right] \quad (5)$$

$$E_{electrostatic} = \sum_{i,j} \frac{1}{4\pi\epsilon_0} \frac{q_i q_j}{r_{ij}} \quad (6)$$

Here k_l , k_θ , and k_n are the force constants for bond stretching, bond angle bending, and torsional force rotations, respectively. l_0 and θ_0 are the equilibrium bond lengths and angles, σ_{ij} and ε_{ij} are the collision distance at which $E_{vdw} = 0$ and potential well depth, respectively. q_i is the atomic charge. l , θ , and φ are the bond lengths, bond angles, and torsional angles, respectively. Force field parameters used in the simulations are summarized below.

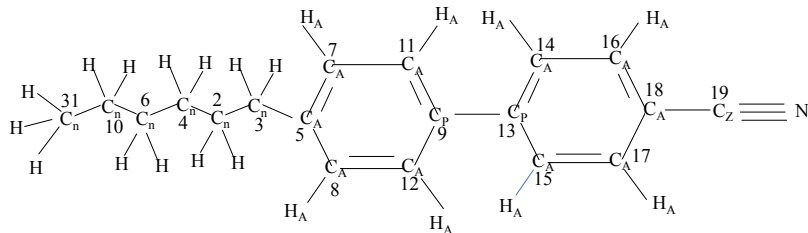


FIG. SM1. Structural details of 6CB molecule. All digits stand for the identity of the atoms. C_A and H_A are aromatic carbon and aromatic hydrogen. C_P is the ring joining carbon atom. C_n and H represent aliphatic carbon and hydrogen. C_z and N_z are the carbon and nitrogen from the cyano group. When we define the atoms using digits as suffix we consider $C_A, C_P, C_n, C_z \equiv C$ or $H_A \equiv H$.

Table 1. Bond stretching force constants (k_l) and equilibrium bond lengths (l_0).

Bond	$k_l(\text{eV } \text{Å}^{-2})$	$l_0(\text{Å})$
C _A -H _A	33.96	1.08
C _A -C _A	44.32	1.38
C _A -C _P	44.32	1.38
C _P -C _P	27.28	1.47
C _A -C _Z	31.52	1.31
C _Z -N _Z	115.11	1.17
C _A -C _n	24.47	1.50
C _n -C _n	22.97	1.51
C _n -HC	31.65	1.09

Table 2. Bond angle bending force constants (k_θ) and equilibrium bond angle (θ_0) for 6CB used in the simulations.

Angle	$k_\theta(\times 10^{-5} \text{ eV/deg}^2)$	$\theta_0(\text{degree})$
C _A -C _A -H _A	98.46	120
C _A -C _A -C _A	84.94	120
C _A -C _P -C _P	95.32	120
C _A -C _A -C _Z	134.38	120
C _A -C _Z -N _Z	71.10	180
C _n -C _n -C _n	244.76	113
C _n -C _n -HC	116.98	112
HC-C _n -HC	147.25	107
C _n -C _A -C _A	185.53	120
C _A -C _n -HC	92.466	109.5
C _A -C _n -C _n	166.44	114

Table 3. Torsional force constants (k_1, k_2, k_3, k_4) for LCs used in simulations.

Torsion	k_1	k_2	k_3	k_4
C _A -C _A -C _A -C _A	0.0	41.240011	0.0	0.0
HC-C _n -C _n -C _n	0.0	0.0	0.16	0.0
HC-C _n -C _n -HC	0.0	0.0	0.14	0.0
C _A -C _P -C _P -C _A	0.0	7.9	0.0	1.76
C _A -C _n -C _n -C _n	3.04000011	0.03000016	-0.1400002	0.54998707
C _n -C _n -C _n -C _n	8.47	0.32	0.12	-1.63
C _A -C _A -C _n -C _n	0.0	3.59	0.0	-0.29

Table 4. Partial charges for all atoms of 6CB molecule used in simulations.

Atom	Charge (e)
Nz	-0.43
C ₁₉	0.395
C ₁₈	0.035
C _{14,15,16,17,11,12,7,8}	-0.122
C _{13,9,5}	0
C _{2,3,4,6,10}	-0.12
C ₃₁	-0.18
H _A	0.122
H	0.06

Table 5. ϵ and σ for all atoms of 6CB molecule used in simulations.

Atom	ϵ (eV)	σ (Å)
Nz	0.00737	3.200
C ₁₉	0.00651	3.650
C ₁₈	0.00304	3.550
C _{14,15,16,17,11,12,7,8}	0.00304	3.550
C _{13,9,5}	0.00304	3.550
C _{2,3,4,6,10}	0.00286	3.500
C ₃₁	0.00286	3.500
H _A	0.001306	2.420
H	0.001306	2.500

Table 6. Partial charges for all atoms of mica surfaces used in simulations. See Ref. 40 in the main text. Same force field parameters are used in Ref. 50 in the main text.

Atom	Charge (e)
K	1.0
Si ^{surface}	1.1
Al ^{surface}	0.8
Al ^{octahedral}	1.45
Mg ^{octahedral}	1.1
O ^{surface}	-0.55
O ^{apical}	-0.758
O ^{hydroxyl}	-0.683
H ^{hydroxyl}	0.2

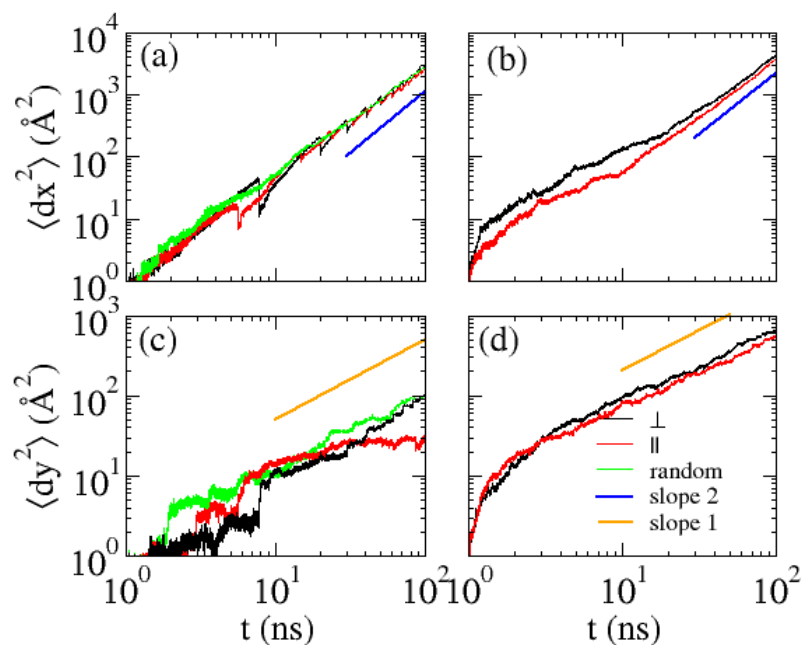


FIG. SM2. Mean square displacement (MSD) of liquid crystals for different surface structures. Left panel is for monolayer and the right panel is for multi-layer lubricant. $\langle dx^2 \rangle$ and $\langle dy^2 \rangle$ are MSD along x and y-direction, respectively.

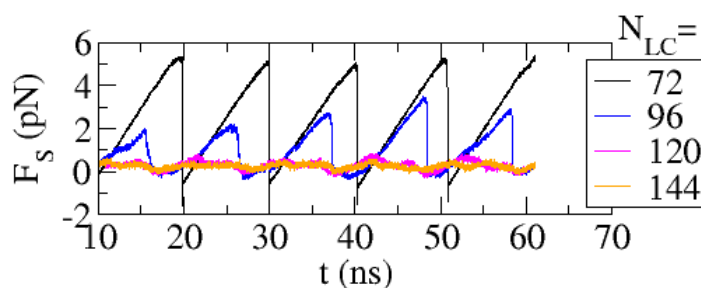


FIG. SM3. Time evolution of friction force F_s is shown with increasing number of liquid crystals, N_{LC} in a pure LC lubricant.

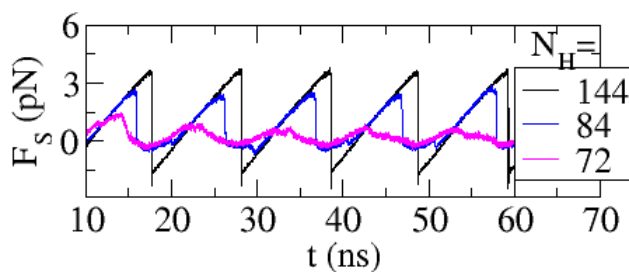


FIG. SM4. Time evolution of friction force F_s is shown for different amount of hexanes N_H in the lubricant mixture. $N_H = 144, 84,$ and 72 correspond to concentrations $\rho_H = 1.0, 0.58,$ and $0.5,$ respectively.

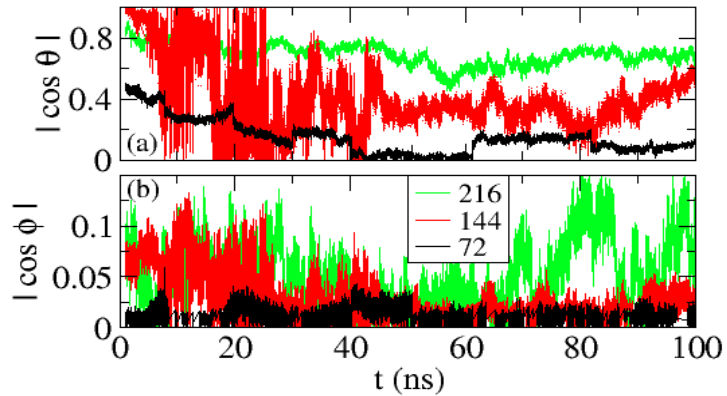


FIG. SM5. Orientation of director field (a) with respect to x-axis, (b) with respect to z-axis for three different systems where the numbers of confined LCs are 216, 144, and 72.

Here, we consider the incommensurate system. To construct the incommensurate setup, we misalign the confining surfaces with respect to each other as shown in Fig. SM6.

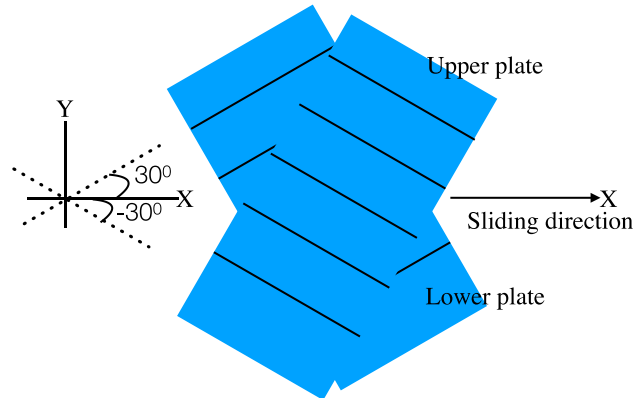


FIG. SM6. Confining plates are misaligned (incommensurate). Grooves from the upper and lower plates make an angle of -30° and $+30^\circ$ with respect to x axis, respectively.

Friction force F_s for the incommensurate case is compared with the commensurate structure, where we probe three different arrangements of ions on the surface (shown in Figure 1 (e), (f), and (g) in the main manuscript), in Fig. SM7.

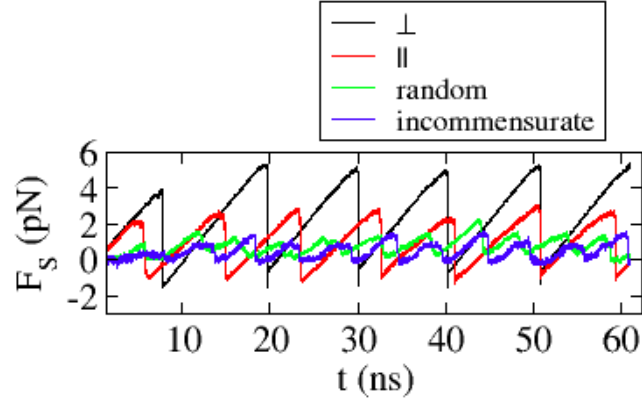


FIG. SM7. Friction force F_s for incommensurate case is compared with commensurate surfaces where we study three different patterns of ions' position on the confining surfaces as shown in Figure 1 (e), (f), and (g) in the main manuscript.

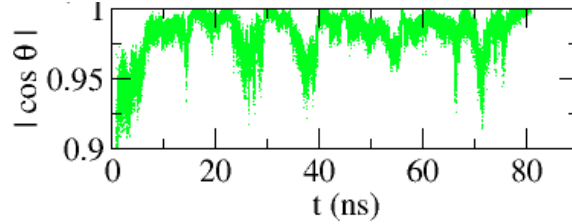


FIG. SM8. Orientation of the director field of LCs where θ is the angle between the director field and the x-axis for misaligned surfaces.

To understand the effect of misaligned surfaces on LCs' orientation we have plotted the alignment of director field in Fig. SM8. In contrast to the commensurate cases, we observe that the director field orients along x axis, not along any of the grooves' direction from two surfaces

In Fig. SM9 we have shown the time evaluation of stick-slip dynamics for the following systems: (a) a mixture of 72 hexane and 72 LCs, and (b) a mixture of 84 hexane and 60 LCs. In the latter case, we see clear slip events in the surface (X_{surface} vs t) and LCs response coherently which is observed in the mean square displacement ($\langle dx^2_{\text{LC}} \rangle$ vs t) plot. However, when slip in the surface is weak, we do not see any response in the LCs.

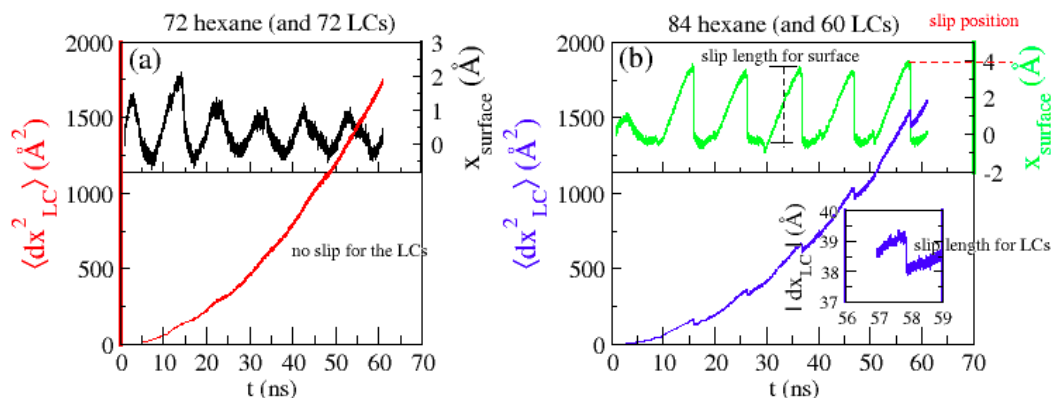


FIG. SM9. Slip in the surface and in the LCs are shown for the following systems: (a) a mixture of 72 hexane and 72 LCs, and (b) a mixture of 84 hexane and 60 LCs. x_{surface} : X component of the center of mass of the lower plate, $\langle dx_{LC}^2 \rangle$: Mean square displacement of LCs along x axis. $|dx_{LC}|$: Average displacement magnitude for LCs along x axis. Slip length is defined as the distance slipped by the center of mass of the lower plate during the motion from the stick to the slip state which is shown as a black dotted line in the top panel of (b).

In Fig. SM10, we characterize the slip events as a function of the amount of hexane. We could not analyze the systems where $\rho_H < 0.5$ because of the disappearance of stick-slip events. It shows that as we increase the amount of hexane starting from equal amount of hexane and LCs mixture, slip length increases and slip happens at a larger displacement of the lower plate.

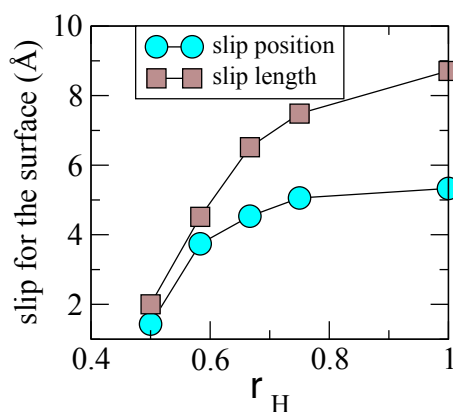


FIG. SM10. Slip in the surface as a function of hexane concentrations.

Title of file: Video SM1

Video caption: Dynamics of 72 liquid crystals forming a monolayer nanoconfined between are not shown in the video for clarity. Color codes of the atoms are same as in Fig. 1 (b).

Title of file: Video SM2

Video caption: Dynamics of 72 liquid crystals forming a monolayer nanoconfined between mica surfaces with grooves orientation parallel to the sliding direction x. Mica surfaces are not shown in the video for clarity. Color codes of the atoms are same as in Fig. 1 (b).

Title of file: Video SM3

Video caption: Dynamics of 72 liquid crystals forming a monolayer nanoconfined between mica surfaces with random occupancy of K^+ ions. Mica surfaces are not shown in the video for clarity. Color codes of the atoms are same as in Fig. 1 (b).

Title of file: Video SM4

Video caption: Dynamics of 216 liquid crystals forming a thicker lubricant layer nanoconfined between mica surfaces. Mica surfaces are not shown in the video for clarity. Color codes of the atoms are same as in Fig. 1 (b).

Title of file: Video SM5

Video caption: Dynamics of a mixture of liquid crystal and hexane (72 LCs and 72 hexanes) nanoconfined between mica surfaces. Mica surfaces are not shown in the video for clarity. Color codes of the atoms are same as in Fig. 1 (b) for 6CB and red colored molecules correspond to hexane.